Nonlinear power spectrum and forecasts for a generalized cubic covariant Galileon

Luís Atayde,[1,*] Noemi Frusciante,[2,†] Benjamin Bose,[3,4,‡] Santiago Casas,[5,§] and Baojiu Li[6,‖]

[1]*Instituto de Astrofisíca e Ciências do Espaço, Faculdade de Ciências da Universidade de Lisboa, Edificio C8, Campo Grande, P-1749016, Lisboa, Portugal*

[2]*Dipartimento di Fisica "E. Pancini," Università degli Studi di Napoli "Federico II," Complesso Universitario di Monte Sant'Angelo, Edificio G, Via Cinthia, I-80126, Napoli, Italy*

[3]*Institute for Astronomy, University of Edinburgh, Royal Observatory, Blackford Hill, Edinburgh, EH9 3HJ, United Kingdom*

[4]*Basic Research Community for Physics e.V., Veddeler Bruckenstrasse 122, 20539 Hamburg, Germany*

[5]*Institute for Theoretical Particle Physics and Cosmology (TTK), RWTH Aachen University, 52056, Aachen, Germany*

[6]*Institute for Computational Cosmology, Department of Physics, Durham University, South Road, Durham, DH1 3LE, United Kingdom*

(Received 25 April 2024; accepted 27 June 2024; published 29 July 2024)

To fully exploit the data from next generation surveys, we need an accurate modeling of the matter power spectrum up to nonlinear scales. Therefore in this work we present the halo model reaction framework for the generalized cubic covariant Galileon (GCCG) model, a modified gravity model within the Horndeski class of theories which extends the cubic covariant Galileon (G3) by including power laws of the derivatives of the scalar field in the K-essence and cubic terms. We modify the publicly available software ReACT for the GCCG in order to obtain an accurate prediction of the nonlinear power spectrum. In the limit of the G3 model we compare the modified ReACT code to N-body simulations and we find agreement within 5% for a wide range of scales and redshifts. We then study the relevant effects of the modifications introduced by the GCCG on the nonlinear matter power spectrum. Finally, we provide forecasts from spectroscopic and photometric primary probes by next generation surveys using a Fisher matrix method. We show that future data will be able to constrain at 1σ the two additional parameters of the model at the percent level and that considering nonlinear corrections to the matter power spectrum beyond the linear regime is crucial to obtain this result.

DOI: 10.1103/PhysRevD.110.024082

I. INTRODUCTION

The observed late-time acceleration of the Universe remains one of the greatest mysteries in cosmology. The standard cosmological model (ΛCDM) assumes the theory of general relativity (GR) to describe the space-time, with the cosmological constant, Λ, being the source of the cosmic acceleration. This model has well known theoretical [1–4] and observational [5–12] shortcomings which motivated the search for models beyond GR, known as modified gravity (MG) models [13].

Scalar-tensor theories are among these MG models and are characterized by an additional scalar field which is coupled to gravity through nonminimal and derivative couplings. Many of these models belong to the Horndeski and/or Galileon theories [14–18]. They have gained a lot of attention given the possibility to construct viable models to account for the late-time acceleration without a cosmological constant as well as to realize phantom dark energy equation-of-state free of ghosts. Additionally in the subclass of Galileon models [19–21] satisfying the constraints on the speed of gravitational waves [22], i.e. $c_{\rm GW} = 1$, there are models for which it has been shown to have a better fit to cosmological data than ΛCDM [23,24]. An example is the generalized cubic covariant Galileon model [25] (GCCG), for which a clear preference over ΛCDM is found when the Planck cosmic microwave background (CMB) temperature and polarization data are used in the analysis [24]. Moreover for this model the value of the today's Hubble parameter, H_0, is found to be consistent with its determination from Cepheids at 1σ [24], resolving the famous tension of the cosmological standard model [8]. In details, the model extends the cubic covariant Galileon (hereafter G3) [16] by including power laws of the field

*Contact author: luisbbatayde@gmail.com
†Contact author: noemi.frusciante@unina.it
‡Contact author: ben.bose@ed.ac.uk
§Contact author: casas@physik.rwth-aachen.de
‖Contact author: baojiu.li@durham.ac.uk

derivatives in the K-essence and cubic terms which still allow for tracker solutions. Contrary to the GCCG, the G3 model has been ruled out by cosmological data [26,27].

While GCCG has been widely studied [24,28] both at background level and linear scales, the nonlinear, small scales are yet to be explored. The nonlinear regime is where the situation starts to become challenging for MG models due to the complexity of the equations to be solved which usually require extremely expensive computations, as well as new phenomenology arising from the screening mechanisms [4] that needs to be taken into account. The latter are mechanisms able to recover GR at Solar System scales where no signature of modifications of the gravitational force has been found (see Ref. [29] for example). In the case of Galileon models it is the Vainshtein mechanism, which acts through the second derivative of the scalar field [30]. Future surveys such as *Euclid*,[1] SKAO[2] and Rubin-LSST,[3] will largely improve the constraints on deviations from GR at these scales. Therefore the physics in the nonlinear regime of cosmic structure formation requires accurate and efficient modeling of nonlinearities and the development of appropriate codes to interpret the data.

In this paper we study the modeling of nonlinearities in the GCCG model using the halo model reaction method [31] which is based on the halo model and perturbation theory, and is implemented in the ReACT code [32–34]. In particular we derive the necessary theoretical quantities and provide the implementation in ReACT. We then use this machinery to forecast how well a spectroscopic survey of galaxies and an imaging survey from a *Euclid*-like mission and SKAO-like one can be used to constrain the GCCG model.

The paper is organized as follows: In Sec. II we review the dynamics of the background evolution and linear growth of perturbations of the GCCG. We also present a detailed study of the collapse of a spherical matter overdensity, the nonlinear growth of large scale structures and the computation of the nonlinear power spectrum at 1-loop order in this model. In Sec. III we revisit the halo model reaction framework and in Sec. IV we validate our approach against N-body simulations. In Sec. V we show the phenomenology of the GCCG model at nonlinear scales and in Sec. VI we provide forecasts for *Euclid*-like and SKAO-like surveys. Finally we conclude in Sec. VII.

II. GENERALIZED CUBIC COVARIANT GALILEON

We start by considering the cubic Horndeski theory described by the action [35,36]

$$S = \int d^4x\sqrt{-g}\left(\frac{M_{\rm pl}^2}{2}R + L_2 + L_3\right) + S_m[g_{\mu\nu},\chi_i], \tag{1}$$

where $M_{\rm pl}^2$ is the Planck mass, R is the Ricci scalar, g is the determinant of the metric $g_{\mu\nu}$, S_m stands for the matter action for all matter fields, χ_i, and the Lagrangians L_i are defined as follows

$$L_2 = G_2(\phi, X), \qquad L_3 = G_3(\phi, X)\Box\phi, \tag{2}$$

with G_i being free functions of the scalar field ϕ and $X = \partial_\mu\phi\partial^\mu\phi$.

In this work we choose the forms of the G_i functions as follows [25]:

$$G_2 = -c_2\alpha_2^{4(1-p_2)}(-X)^{p_2}, \quad G_3 = -c_3\alpha_3^{1-4p_3}(-X)^{p_3}, \tag{3}$$

where c_i and p_i are dimensionless constants and α_i are constants with dimensions of mass, defined as

$$\alpha_2 = \sqrt{H_0 M_{\rm pl}}, \qquad \alpha_3 = \left(\frac{M_{\rm pl}^{1-2p_3}}{H_0^{2p_3}}\right)^{\frac{1}{1-4p_3}}, \tag{4}$$

with H_0 being the Hubble constant. Without loss of generality we set $c_2 = 1/2$ [26,37,38]. The above model is known to be the generalized cubic covariant Galileon (hereafter GCCG) and it extends the original proposal of the covariant Galileon [16] (hereafter G3) because it considers power law functions of X in the Lagrangians, i.e. $G_i \propto X^{p_i}$. Indeed the G3 model is obtained by setting $p_2 = p_3 = 1$.

A. Background evolution

At background level if we consider the flat Friedmann-Lemaître-Robertson-Walker (FLRW) metric

$$ds^2 = -N(t)dt^2 + a^2(t)\delta_{ij}dx^i dx^j, \tag{5}$$

where $a(t)$ is the scale factor, $N(t)$ is the lapse function and t is the cosmic time, we can vary Eq. (1) with respect to a and N and we obtain

$$3M_{\rm pl}^2H^2 = (\rho_{\rm m} + \rho_\phi), \tag{6}$$

$$M_{\rm pl}^2(2\dot{H} + 3H^2) = -(p_{\rm m} + p_\phi), \tag{7}$$

where $H \equiv \dot{a}/a$ is the Hubble rate, an over-dot stands for derivatives with respect to t, $\rho_{\rm m}$ and $p_{\rm m}$ are the density and pressure of the standard matter fluids and

$$\rho_\phi = 2XG_{2,X} - G_2 - 6aXH\phi' G_{3,X} - XG_{3,\phi}, \tag{8}$$

$$p_\phi = G_2 + 2X(a(\dot{H}+H^2)\phi' - a^2H^2\phi'')G_{3,X} - XG_{3,\phi}, \tag{9}$$

[1]*Euclid*: www.euclid-ec.org.
[2]Square Kilometer Array Observatory: https://www.skao.int.
[3]The Vera C. Rubin Observatory Legacy Survey of Space and Time: https://www.lsst.org.

are the density and pressure associated to the scalar field. Here the prime is the derivative with respect to the scale factor, $G_{i,X} = \partial G_i/\partial X$ and $G_{i,\phi} = \partial G_i/\partial\phi$. For the matter fields, which we assume to be perfect fluids, we consider the continuity equation:

$$\dot{\rho}_{\rm m} + 3H(1+w)\rho_{\rm m} = 0, \tag{10}$$

with $w \equiv p_{\rm m}/\rho_{\rm m}$. Finally, the equation of evolution for ϕ can be obtained by varying Eq. (1) with respect to the scalar field itself. It reads

$$\frac{H}{a^2}\frac{\rm d}{{\rm d}a}(a^3 J) = P, \tag{11}$$

where

$$J = -2aH\phi' G_{2,X} - 6HXG_{3,X} + 2aH\phi' G_{3,\phi}, \tag{12}$$

$$P = G_{2,\phi} - 2X\{G_{3,\phi\phi} - 2[a(\dot{H}+H^2)\phi' - a^2H^2\phi'']G_{3,\phi X}\}. \tag{13}$$

The GCCG model at the background level is characterized by a tracker solution which is given by [25]

$$H^{2q+1}\psi^{2q} = \zeta H_0^{2q+1}, \tag{14}$$

where we have defined a dimensionless constant

$$q \equiv (p_3 - p_2) + \frac{1}{2}, \tag{15}$$

and a dimensionless scalar field

$$\psi \equiv \frac{1}{M_{\rm pl}}\frac{d\phi}{d\ln a}. \tag{16}$$

We have also introduced a dimensionless constant ζ. We can implement the above tracker solution in the background Eq. (6), which simply reads [24]

$$\left(\frac{H}{H_0}\right)^{2+s} = \Omega_\phi^0 + \left[\frac{\Omega_c^0+\Omega_b^0}{a^3} + \frac{\Omega_r^0}{a^4}\right]\left(\frac{H}{H_0}\right)^s, \tag{17}$$

where $s = p_2/q$ and $\Omega_i^0 \equiv \rho_i^0/3M_{\rm pl}^2H_0^2$ is the density parameter at present time for cold dark matter, c, baryonic matter, b, radiation, r, and scalar field, ϕ. The latter can be computed by evaluating the above equation at the present time, which gives the flatness condition

$$\Omega_\phi^0 = 1 - \Omega_{\rm m}^0 = c_3(2sq+2q-1)\zeta^{s+1} - \frac{1}{6}(2sq-1)\zeta^s, \tag{18}$$

where $\Omega_{\rm m}^0 = \Omega_c^0 + \Omega_b^0 + \Omega_r^0$. It can be easily verified that

$$\zeta = (6\Omega_\phi^0)^{\frac{1}{s}}, \qquad c_3 = \frac{1}{3}\frac{sq}{(6\Omega_\phi^0)^{\frac{1}{s}}(2sq+2q-1)}, \tag{19}$$

therefore the GCCG model has only two extra free parameters, i.e. $\{s, q\}$, with respect to ΛCDM. In this description the G3 model does not have additional parameters because $s = 2$ and $q = 1/2$. The GCCG model has been analyzed using data by *Planck* and it has been found at 95% CL that $q > 0$ and $s = 0.6^{+1.7}_{-0.6}$ and a preference over ΛCDM has been found using the effective $\chi^2_{\rm eff}$ and deviance information criterion [24]. Including the measurements of baryon acoustic oscillation, SNIa and redshift space distortion is possible to find a lower bound for q, i.e. $q > 0.8$, while $s = 0.05^{+0.08}_{-0.05}$. We note that due to stability conditions (ghost and gradient requirements) both parameters are restricted to be positive.

B. Linear growth of perturbations

At the linear perturbation level we can consider the perturbed FLRW metric in the Newtonian gauge[4]

$${\rm d}s^2 = -(1+2\Psi){\rm d}t^2 + a^2(1-2\Phi)\delta_{ij}{\rm d}x^i{\rm d}x^j, \tag{20}$$

where $\Phi(t, x_i)$ and $\Psi(t, x_i)$ are the two gravitational potentials. We can write general forms for the linear perturbation equations in MG which relate the gravitational potentials and the matter perturbation $\delta_{\rm m} \equiv \delta\rho_{\rm m}/\rho_{\rm m}$, where $\rho_{\rm m}$ is the background matter density. They are [40–44]:

$$-k^2\Psi = 4\pi G_{\rm N}a^2\mu_{\rm L}(a,k)\rho_{\rm m}\delta_{\rm m}, \tag{21}$$

$$-k^2(\Psi+\Phi) = 8\pi G_{\rm N}a^2\Sigma_{\rm L}(a,k)\rho_{\rm m}\delta_{\rm m}, \tag{22}$$

where k is the comoving wavenumber, $G_{\rm N} = (8\pi M_{\rm pl}^2)^{-1}$ is the Newtonian gravitational constant, μ_L and Σ_L are respectively the linear effective gravitational coupling and light deflection parameter. For the GCCG model, when using the Quasi Static Approximation (QSA)[5] they read:

$$\mu_L(a) = \left(1 + \frac{2\alpha_B^2}{c_s^2\alpha}\right), \qquad \Sigma_L(a) = \mu_L, \tag{23}$$

[4]We note that the definition of the metric in Ref. [39] uses an opposite convention: $\delta g_{00} = 2\Phi$ and $\delta g_{ij} = -2\Psi\delta_{ij}$. For the model under consideration we will see that $\Phi = \Psi$.

[5]The QSA assumes that the time derivatives of the perturbed quantities can be neglected when compared with their spatial derivatives. This approximation is valid for modes deep inside the Hubble radius [45].

with $\alpha \equiv \alpha_K + 6\alpha_B^2 > 0$ being the no-ghost condition with

$$\alpha_K = -12q\alpha_B, \qquad \alpha_B = -sq\Omega_\phi^0\left(\frac{H_0}{H}\right)^{s+2}, \quad (24)$$

being respectively the kineticity and the braiding functions. Finally, c_s^2 is the speed of propagation of the scalar mode and it is defined as

$$c_s^2 = \frac{2}{\alpha}\left[(1+\alpha_B)\left(-\frac{\dot{H}}{H^2}-\alpha_B\right)-\frac{\dot{\alpha_B}}{H}\right]-\frac{3\Omega_m}{\alpha}. \quad (25)$$

The latter has to be positive to avoid gradient instability. For a thorough discussion about the viability space of the GCCG model we forward the reader to Refs. [24,28].

Finally we have to consider the evolution equation of the matter density perturbation which reads

$$\frac{d^2\delta_m}{d^2\ln a}+\left(2+\frac{1}{H}\frac{dH}{d\ln a}\right)\frac{d\delta_m}{d\ln a}-\frac{3}{2}\Omega_m\mu_L(a)\delta_m=0, \quad (26)$$

where $\Omega_m(a) = \rho_m/3M_{pl}^2H^2$ is the time dependent matter density parameter.

C. Nonlinear growth of perturbations

Let us consider nonlinear perturbations and assume the QSA holds. We will consider for modeling the formation of gravitationally bound structures, the spherical collapse model to describe the collapse of what we assume to be a spherical overdensity. The collapse phase is then followed by a phase where virialization takes place. The methodology adopted here has been already applied to MG models [46–53].

The nonlinear equations for the GCCG model read [53]

$$\nabla^2\Psi = \frac{\rho\delta_m}{2M_{pl}^2}+\alpha_B\nabla^2Q, \quad (27)$$

$$\Phi = \Psi, \quad (28)$$

$$\nabla^2Q+\frac{\lambda^2}{H}[(\nabla_i\nabla_jQ)^2-(\nabla^2Q)^2] = -\frac{\lambda^2H}{2M_{pl}^2}\rho\delta_m, \quad (29)$$

where we have defined

$$Q = \frac{H\delta\phi}{\dot{\phi}}, \qquad \lambda^2 = -\frac{2\alpha_B}{H\alpha c_s^2}. \quad (30)$$

Combining the above equations, assuming a top-hat profile for the density field and after some integrations, we found a modified Poisson equation which includes nonlinear corrections

$$\frac{\partial^2\Psi}{a^2} = 4\pi G_N\mu^{NL}(a,R)\rho_m\delta_m, \quad (31)$$

where we define μ^{NL} as the nonlinear effective gravitational coupling and its form is

$$\mu^{NL}(a,R) = 1+2(\mu^L-1)\left(\frac{R}{R_V}\right)^3\left(\sqrt{1+\frac{R_V^3}{R^3}}-1\right), \quad (32)$$

with

$$\left(\frac{R_V}{R}\right)^3 = 4H_0^2\Omega_m^0\lambda^4\frac{\delta_m}{a^3}, \quad (33)$$

where $R_V^3 = 8G_N\lambda^4\delta M$ is the Vainshtein radius, δM being the total mass of the density perturbation $\delta\rho_m$ and R is the radius of the sphere of mass M. The Vainshtein mechanism plays a very important role when considering the formation of gravitationally bound structures. Indeed it suppresses the modification to the gravitational force in high-density environments which is what happens during the collapse phase when the density of the region is sufficiently high to significantly modify the dynamics of the scalar field.

1. Spherical collapse

The general form of the nonlinear evolution equation for the matter density is

$$\ddot{\delta}_m + 2H\dot{\delta}_m - \frac{4}{3}\frac{\dot{\delta}_m^2}{1+\delta_m} = (1+\delta_m)\frac{\partial^2\Psi}{a^2}, \quad (34)$$

which for MG assumes the following form when the Poisson equation is used

$$\ddot{\delta}_m + 2H\dot{\delta}_m - \frac{4}{3}\frac{\dot{\delta}_m^2}{1+\delta_m} = 4\pi G_N\mu^{NL}\rho_m(1+\delta_m)\delta_m. \quad (35)$$

The above equation can be used to obtain the equation for the radius of the spherical top-hat, R, by starting from the assumption that the total mass inside R is conserved during the collapse phase, i.e.

$$M = \frac{4\pi}{3}R^3\rho_m(1+\delta_m) = \text{const.} \quad (36)$$

By performing a change of variable

$$y = \frac{R}{R_i}-\frac{a}{a_i}, \quad (37)$$

where R_i and a_i are respectively the initial values of R and scale factor, and differentiating Eq. (36), one finds

$$\frac{d^2y}{d\ln a^2} = -\frac{1}{H}\frac{dH}{d\ln a}\frac{dy}{d\ln a}+\left(1+\frac{1}{H}\frac{dH}{d\ln a}\right)y - \frac{\Omega_m}{2}\mu^{NL}\delta_m\left(y+\frac{a}{a_i}\right). \quad (38)$$

Finally, we can write the overdensity as

$$\delta_{\rm m} = (1+\delta_{{\rm m},i})\left(1+\frac{a_i}{a}y\right)^{-3} - 1, \tag{39}$$

which follows from matter conservation.

2. Virial theorem

Finally we consider the last stage of the collapse: the virialization, i.e. when the collapse stops and the system reaches equilibrium, and satisfies the virial theorem. The virial theorem reads

$$W + 2T = 0, \tag{40}$$

where W is the potential energy and T the kinetic energy. The kinetic energy has the form

$$\frac{T}{E_0} = \frac{H^2}{H_0^2}\left[\frac{a}{a_i}\left(\frac{{\rm d}y}{{\rm d}\ln a}+y\right)\right]^2, \tag{41}$$

with $E_0 = 3/10M(H_0R_i)^2$. The potential energy gets three energy contributions: the Newtonian (W_N), scalar field (W_ϕ) and background ($W_{\rm eff}$) potential energies, which read [31,46]

$$\frac{W_N}{E_0} = -\Omega_{\rm m}^0 y^2(1+\delta_{\rm m})\frac{a^{-1}}{a_i^2}, \tag{42}$$

$$\frac{W_\phi}{E_0} = -\Omega_{\rm m}^0 \mathcal{F} y^2 \delta_{\rm m}\frac{a^{-1}}{a_i^2}, \tag{43}$$

$$\frac{W_{\rm eff}}{E_0} = -\frac{8\pi G_N}{3H_0^2}(1+3w_{\rm eff})\bar{\rho}_{\rm eff}\frac{a^2}{a_i^2}y^2, \tag{44}$$

where for the GCCG we have defined $\mathcal{F} \equiv \mu^{NL} - 1$ in Eq. (32) and

$$\bar{\rho}_{\rm eff} = \left(\frac{H_0}{H}\right)^s \frac{3H_0}{8\pi G_N}\Omega_\phi^0, \tag{45}$$

$$w_{\rm eff} = \frac{\dot{H}s}{3H^2} - 1, \tag{46}$$

according to which

$$\frac{W_{\rm eff}}{E_0} = \left(2 - \frac{\dot{H}}{H^2}s\right)\left(\frac{H}{H_0}\right)^2(1-\Omega_{\rm m})\frac{a^2}{a_i^2}y^2. \tag{47}$$

3. Higher order coupling kernels of the power spectrum at 1-loop order

In this section we compute the nonlinear power spectrum at 1-loop order using standard perturbation theory (SPT) [54]. We consider the relation between Ψ and $\delta_{\rm m}$ and expand up to 3rd order in the matter perturbation [55,56]

$$-\frac{k^2}{a^2H^2}\Psi = \frac{3}{2}\Omega_{\rm m}\mu_L(k,a)\delta_{\rm m}(\mathbf{k}) + S(\mathbf{k}), \tag{48}$$

where $S(\mathbf{k})$ is the nonlinear source term up to the third order and it is given by [57]

$$\begin{aligned} S(\mathbf{k}) = &\int \frac{d^3\mathbf{k}_1 d^3\mathbf{k}_2}{(2\pi)^3}\delta_D(\mathbf{k}-\mathbf{k}_{12})\gamma_2(\mathbf{k},\mathbf{k}_1,\mathbf{k}_2;a)\delta_{\rm m}(\mathbf{k}_1)\delta_{\rm m}(\mathbf{k}_2) \\ &+ \int \frac{d^3\mathbf{k}_1 d^3\mathbf{k}_2 d^3\mathbf{k}_3}{(2\pi)^6}\delta_D(\mathbf{k}-\mathbf{k}_{123})\gamma_3(\mathbf{k},\mathbf{k}_1,\mathbf{k}_2,\mathbf{k}_3;a)\delta_{\rm m}(\mathbf{k}_1)\delta_{\rm m}(\mathbf{k}_2)\delta_{\rm m}(\mathbf{k}_3), \end{aligned} \tag{49}$$

where δ_D is the Dirac delta function, $\mathbf{k}_{ij} = \mathbf{k}_i + \mathbf{k}_j$ and $\mathbf{k}_{ijk} = \mathbf{k}_1 + \mathbf{k}_j + \mathbf{k}_k$, $\gamma_2(\mathbf{k},\mathbf{k}_1,\mathbf{k}_2;a)$ and $\gamma_3(\mathbf{k},\mathbf{k}_1,\mathbf{k}_2,\mathbf{k}_3;a)$ are functions symmetric under the exchange of $\mathbf{k}_i$. We follow Ref. [57] to compute their forms for the GCCG and we find

$$\gamma_2(\mathbf{k},\mathbf{k}_1,\mathbf{k}_2;a) = -18\left(\frac{H_0}{H}\right)^4\frac{\alpha_B^4}{(\alpha c_s^2)^3}\left(\frac{\Omega_{\rm m}^0}{a^3}\right)^2\left(1-\frac{(\mathbf{k}_1\cdot\mathbf{k}_2)^2}{k_1^2k_2^2}\right), \tag{50}$$

$$\gamma_3(\mathbf{k},\mathbf{k}_1,\mathbf{k}_2,\mathbf{k}_3;a) = 72\left(\frac{H_0}{H}\right)^6\frac{\alpha_B^6}{(\alpha c_s^2)^5}\left(\frac{\Omega_{\rm m}^0}{a^3}\right)^3\left(1-\frac{(\mathbf{k}_1\cdot\mathbf{k}_{23})^2}{k_1^2k_{23}^2}\right)\left(1-\frac{(\mathbf{k}_2\cdot\mathbf{k}_3)^2}{k_2^2k_3^2}\right). \tag{51}$$

III. THE HALO MODEL REACTION

In this section we review a model-independent framework to compute the nonlinear matter power spectrum, namely the halo model reaction [31]. This approach combines both 1-loop perturbation theory and the halo model.

The nonlinear matter power spectrum of a modified theory of gravity, hereafter $P_{\rm NL}$, is computed as follows

$$P_{\rm NL} = \mathcal{R}(k,z)P_{\rm NL}^{\rm pseudo}(k,z), \tag{52}$$

where $P_{\rm NL}^{\rm pseudo}$ is the nonlinear pseudo power spectrum. This is a the nonlinear matter power spectrum within ΛCDM whose initial conditions are such that the modified linear clustering is reproduced at the target redshift. The second component, $\mathcal{R}$, is the halo model reaction given by

$$\mathcal{R}(k,z)=\frac{\{[1-\mathcal{E}(z)]e^{-k/k_\star(z)}+\mathcal{E}(z)\}P_{\rm L}(k,z)+P_{\rm 1h}(k,z)}{P_{\rm hm}^{\rm pseudo}(k,z)}, \tag{53}$$

with $P_{\rm L}$ being the MG linear matter power spectrum and $P_{\rm 1h}$ being the 1-halo contribution to the power spectrum as predicted by the halo model for the MG scenario (see Sec. II C 1 for the GCCG case). Finally we have

$$P_{\rm hm}^{\rm pseudo}(k,z)=P_{\rm L}(k,z)+P_{\rm 1h}^{\rm pseudo}(k,z), \tag{54}$$

$$\mathcal{E}(z)=\lim_{k\to 0}\frac{P_{\rm 1h}(k,z)}{P_{\rm 1h}^{\rm pseudo}(k,z)}, \tag{55}$$

$$k_\star(z)=-\bar{k}\left\{\ln\left[\frac{A(\bar{k},z)}{P_{\rm L}(\bar{k},z)}-\mathcal{E}(z)\right]-\ln[1-\mathcal{E}(z)]\right\}^{-1}, \tag{56}$$

where $\bar{k}=0.06\ h\,{\rm Mpc}^{-1}$ and the $k\to 0$ limit in the above is taken to be $k=0.01\ h\,{\rm Mpc}^{-1}$ according to Ref. [31] and

$$A(k,z)=\frac{P_{\rm 1-loop}(k,z)+P_{\rm 1h}(k,z)}{P_{\rm 1-loop}^{\rm pseudo}(k,z)+P_{\rm 1h}^{\rm pseudo}(k,z)}P_{\rm hm}^{\rm pseudo}(k,z) - P_{\rm 1h}(k,z). \tag{57}$$

In the above expressions we further define $P_{\rm 1h}^{\rm pseudo}$ as the 1-halo contribution to the power spectrum as predicted by the halo model for the pseudocosmology, $P_{\rm 1-loop}$ and $P_{\rm 1-loop}^{\rm pseudo}$ are respectively the 1-loop matter power spectra from SPT with and without nonlinear MG effects ($S(\mathbf{k})=0$). The higher order coupling kernels of $P_{\rm 1-loop}$ for the GCCG model are calculated in Sec. II C 3.

We modify the public software package ReACT [32,33] which allows for fast and accurate calculation of nonlinear power spectra for beyond standard models using the reaction method reviewed above. Our new patch accounts for a modified background evolution [Eq. (17)], the spherical collapse and virial theorem computations defined respectively in Secs. II C 1 and II C 2, which are needed for the halo-model spectra computations, and the 1-loop corrections in Sec. II C 3 to compute the 1-loop matter power spectra. Note our implementation also allows the computation of the redshift space power spectrum multipoles in GCCG [57].

We have compared the background evolution and the linear matter power spectrum of the GCCG of our ReACT patch with the Einstein-Boltzmann solver EFTCAMB [58,59] where the GCCG is implemented [24], and we find agreement at the subpercent level. For the nonlinear matter power spectrum implementation we discuss its validation in the next section.

Note that for the nonlinear spectrum, we must also choose a prescription for $P_{\rm NL}^{\rm pseudo}$ in Eq. (52). For this we make two choices in the draft: HALOFIT [60] and HMCode2020 [61]. We would normally expect HMCode2020 to be the most accurate prescription, but what we have found is that this prescription gives poor results when comparing Eq. (52) directly with the simulation measurements. This is likely due to the exceptionally high $\sigma_8(z=0)$ of the simulations, which is far beyond the values to which HMCode2020 was fit to. Further, it was found that the HMCode2020-based nonlinear boost factor, $B(k,z)=\mathcal{R}(k,z)\times P_{\rm HMCode2020}^{\rm pseudo}(k,z)/P_{\rm HMCode2020}^{\Lambda\rm CDM}\leq 1$ at quasi-nonlinear scales. This is not to be expected from such scalar tensor theories which act to enhance power. This effect was not found for HMCode2016 nor HALOFIT.

In particular, HMCode2020 introduces a σ_8 dependent damping to the linear power spectrum which can cause exactly this effect, as well as over damping of the power spectrum if σ_8 is exceptionally high, as in the simulations considered in this work. For this reason, we choose to use halofit when comparing to the simulations which gives the level of agreement seen in many other works [31–33,62–67]. In our forecasts, we switch to HMCode2020 as the fiducial σ_8 is chosen to be much lower, where the HMCode2020 prescription for the pseudospectrum should outperform HALOFIT. In an upcoming work we demonstrate this improvement explicitly.

IV. VALIDATION OF THE MODELING AGAINST SIMULATIONS

N-body cosmological simulations of the GCCG do not exist yet but in the limit $s=2$ and $q=1/2$ the model reduces to the G3 model for which simulations were run using the ECOSMOG code [49,68,69]. We will employ these simulations to validate our implementation of the nonlinear matter power spectrum in the G3 limit. The simulations are dark matter only and the box sizes are $L=200\ {\rm Mpc}\,h^{-1}$ and $L=400\ {\rm Mpc}\,h^{-1}$ with threshold values $N_{\rm p,th}=8$ and $N_{\rm p,th}=6$ respectively. In both cases the total number of particles is $N_{\rm p}=512^3$ and the domain grid has 512 cells in each direction. The reference cosmology for these simulations considers the best fits obtained by running Monte Carlo Markov chains and combining WMAP9 + SNLS + BAO data [70]: $\Omega_{\rm r}^0h^2=4.28\times10^{-5}$, $\Omega_{\rm b}^0h^2=0.02196$, $\Omega_{\rm c}^0h^2=0.1274$, $h=H_0/100=0.7307$, the primordial spectra index $n_{\rm s}=0.953$, the optical depth to reionization $\tau=0.0763$, the scalar amplitude $A_{\rm s}$ at pivot scale $k=0.02\ {\rm Mpc}^{-1}$ is $\log[10^{10}A_{\rm s}]=3.154$. The background is solved differently than our approach, where $c/c_3^{2/3}=-5.378$ and $c_3=10$ and $\log[\rho_{\phi,i}/\rho_{m,i}]=-4.22$,

where "i" refers to quantities evaluated at initial time, $z_i = 10^6$. We adopt the same values for the cosmological parameters for comparison purposes but note that $\Omega_r^0 = 0$ is assumed in ReACT.

Besides the simulations for the G3 model, in the same work the authors run simulations for another model, QCDM, which is defined such that the background is the same as G3 and the perturbations are those of ΛCDM. This was made with the purpose of disentangling the effects of the modified gravitational strength in changing the linear matter growth from those of the background. We have also implemented this scenario in our ReACT patch.

In Figs. 1 and 2 we present the results of the comparison for QCDM and the G3 models respectively. We show results for both the pseudo spectra and full h alo model reaction predictions along with the matter power spectra measured from the N-body simulations for three different times ($a = 0.60$, 0.80, 1 or $z = 0.67$, 0.25, 0) and for box size $L = 400\,\mathrm{Mpc}\,h^{-1}$. From Fig. 1 we can infer differences coming from the background evolution only. Let us stress that the N-body simulations and the theoretical predictions use different approaches to solve the background evolution which can lead to small differences. Despite this, for all three scale factors, we have agreement between theory and simulation within 5% for $2\times10^{-2}\,h\,\mathrm{Mpc}^{-1} \lesssim k \lesssim 1\,h\,\mathrm{Mpc}^{-1}$. Further, for $0.2\,h\,\mathrm{Mpc}^{-1} \lesssim k \lesssim 0.7\,h\,\mathrm{Mpc}^{-1}$ the agreement is better (within 3%). For the G3 model the accuracy is the same as for QCDM (see Fig. 2). For the reaction predictions it is even possible to find agreement within the 5% region for smaller scales ($k \lesssim 3\,h\,\mathrm{Mpc}^{-1}$ at $a = 0.6$ and $a = 0.8$ and $k \lesssim 5\,h\,\mathrm{Mpc}^{-1}$ at $a = 1$).

Recall that the accuracy of our pseudospectrum, HALOFIT, is ∼5% at these scales [60], implying improvement in the pseudo can lead to far better predictions. Slightly better accuracy (∼2–3%) was found for many other nonstandard models within the halo model reaction formalism [31,33,62–65,67,71] where the authors typically compare the theoretical predictions to simulation measurements of the ratio of power spectra with respect to ΛCDM, which are not available in this case. The ratio typically factors out some of the systematic inaccuracy of the pseudo.

We thus conclude that our predictions show the expected accuracy of the halo model reaction formalism as presented in the literature, which we deem sufficient up to scales $k \lesssim 1\,h\,\mathrm{Mpc}^{-1}$ for a wide redshift range, and that the reaction formalism can then be used to model the nonlinearities of the Galileon model. We then extend the validity of the modeling to the GCCG as well.

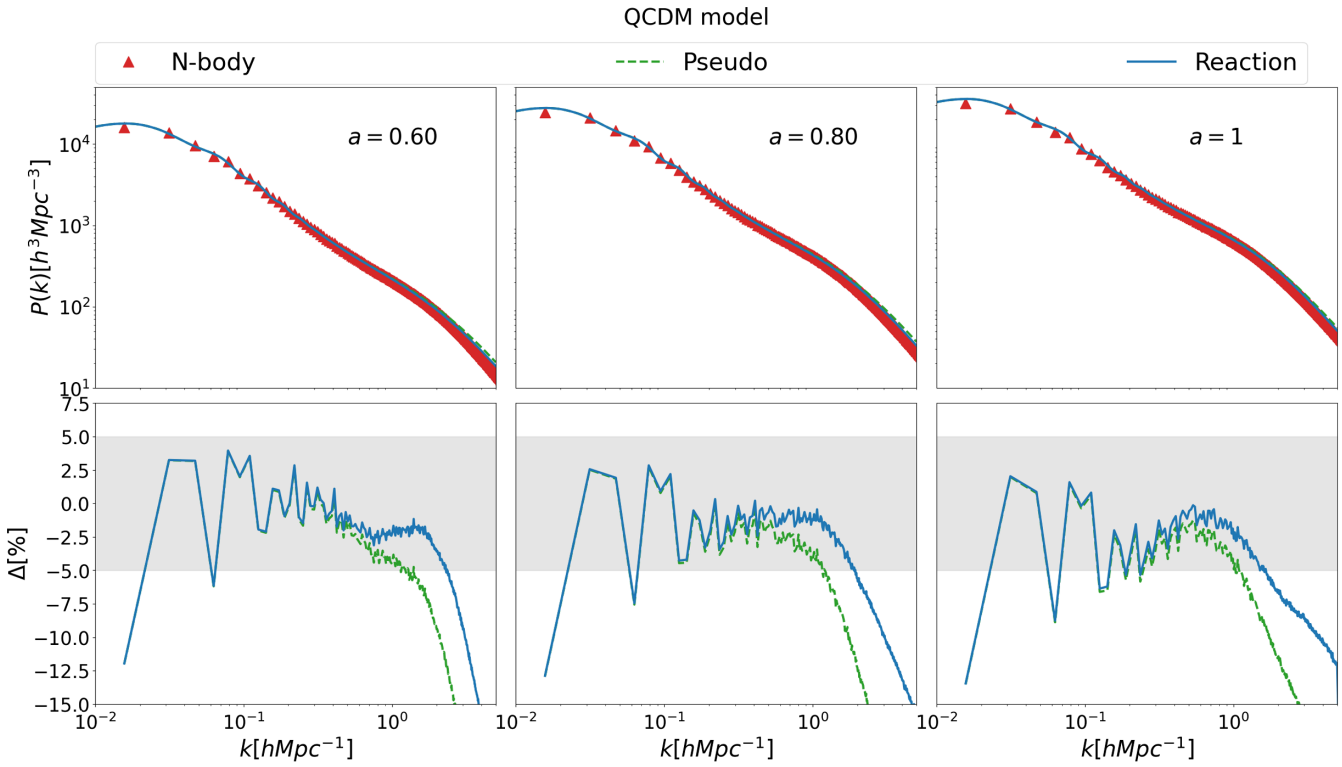

FIG. 1. Top panels: nonlinear matter power spectra for the QCDM model at three times: $a = 0.60$, 0.80 and 1. Red triangles are measurements from the N-body simulations, green dashed lines are the pseudo spectrum and blue solid lines are the halo model reaction predictions. Bottom panels: relative percentage difference of the model predictions vs N-body simulations for the nonlinear matter power spectra, $\Delta = 100\%(1 - P_{\mathrm{prediction}}/P_{\mathrm{N-body}})$.

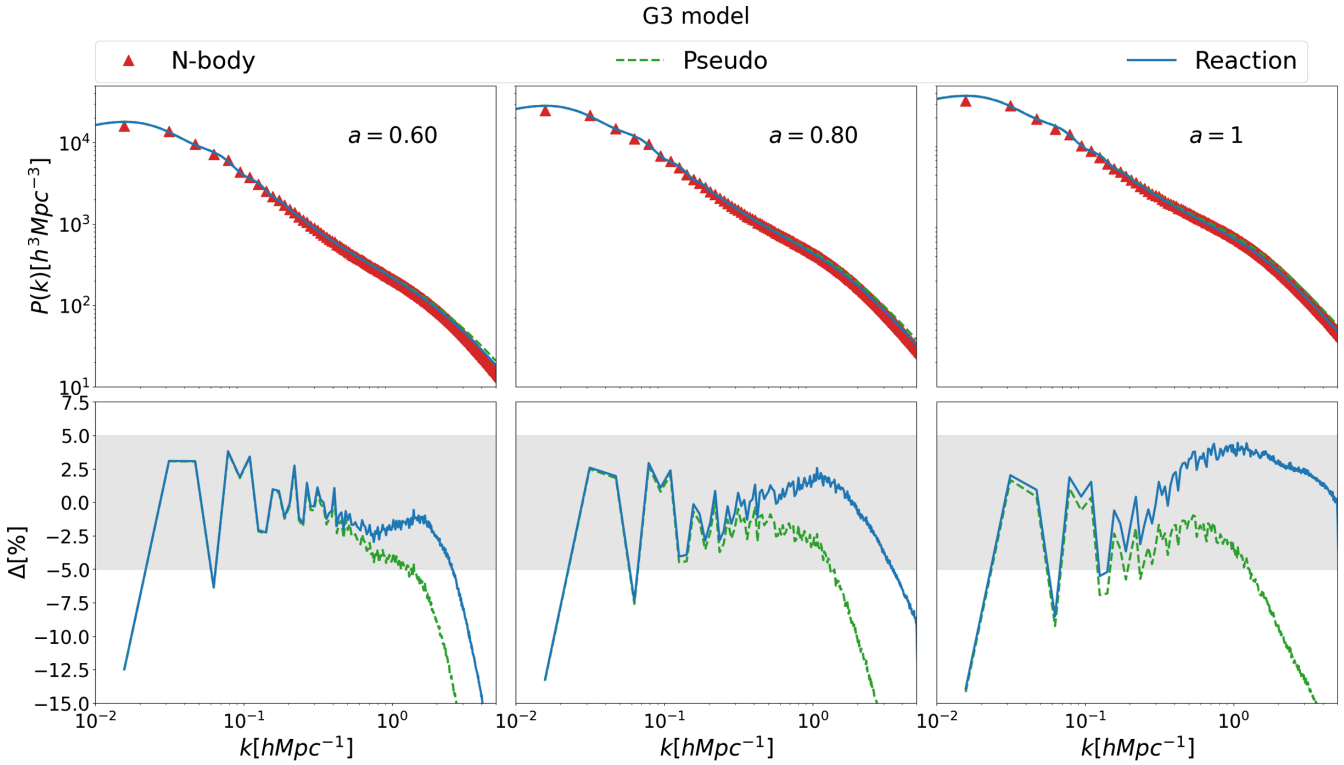

FIG. 2. Top panels: nonlinear matter power spectra for the G3 model at three times: $a = 0.60$, 0.80 and 1. Red triangles are measurements from the N-body simulations, green dashed lines are the pseudospectrum and blue solid lines are the halo model reaction predictions. Bottom panels: relative percentage difference of the model predictions vs N-body simulations for the nonlinear matter power spectra, $\Delta = 100\%(1 - P_{\rm prediction}/P_{\rm N-body})$.

V. PHENOMENOLOGY OF THE NONLINEAR MATTER POWER SPECTRUM FOR GENERALIZED CUBIC COVARIANT GALILEON

In this section we illustrate the phenomenology of the GCCG by considering the nonlinear matter power spectrum predictions from ReACT. In order to quantify the deviation with respect to the standard scenario and to the linear behavior, we consider two sets of values for $\{s, q\}$: $\{s = 2, q = 0.35\}$, we refer to it as GCCG1 and $\{s = 1.3, q = 0.5\}$, hereafter GCCG2. For comparison we include also G3 ($\{s = 2, q = 0.5\}$). For the cosmological parameters we use the same as in previous section. We show in Fig. 3 the ratio of the linear (solid lines) and nonlinear (dashed lines) matter power spectra for the Galileon models with respect to their ΛCDM counterparts at $z = 0$. We note at linear scales an enhancement of the growth of structure with respect to ΛCDM for $0.01\ h\,\mathrm{Mpc}^{-1} \lesssim k \lesssim 0.1\ h\,\mathrm{Mpc}^{-1}$. The enhancement is larger for the models with the higher values of s, i.e., G3 (green solid lines) and GCCG1 (blue solid lines). GCCG1 power spectra are lower than G3 ones because the value of q is smaller. We can also notice that up to $k \lesssim 0.1\ h\,\mathrm{Mpc}^{-1}$ there is good agreement between the nonlinear and the linear theory prediction ($\lesssim$0.5%). We can then deduce that the screening mechanism does not affect the large scales where usually the validity of the linear perturbation theory is assumed. Nonlinear corrections enter at smaller scales ($k \gtrsim 0.1\ h\,\mathrm{Mpc}^{-1}$). We observe up to a ∼4% enhancement for $0.1\ h\,\mathrm{Mpc}^{-1} \lesssim k \lesssim 1\ h\,\mathrm{Mpc}^{-1}$

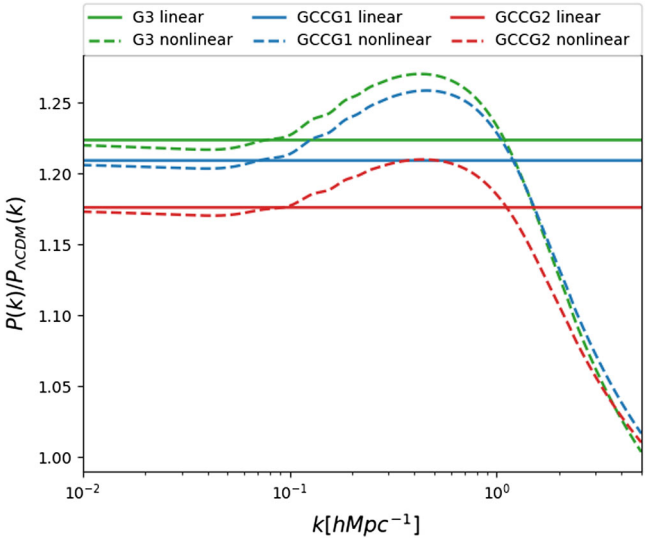

FIG. 3. Ratio of the linear (solid lines) and nonlinear (dashed lines) matter power spectra for the Galileon models with respect to their ΛCDM counterparts.

with respect to linear ratio and finally for the higher k a suppression, showing the efficiency of the screening mechanism. We note that we do not expect the ratio to go to unity as $k \to \infty$. In this case, the Poisson equation will approach the GR expression, but the perturbations will still be modified with respect to ΛCDM as they will experience a GCCG background expansion.

VI. FORECASTS ANALYSIS FOR SPECTROSCOPIC AND PHOTOMETRIC PRIMARY PROBES

We will provide forecasts for the GCCG model using spectroscopic and photometric galaxy clustering (GC_{sp} and GC_{ph}) and weak lensing (WL) probes. We will also include the cross correlation of GC_{ph} and WL (we will refer to this combination as XC) as well as the full combination of probes. We will use specifications of surveys such as *Euclid*-like and SKAO-like. We selected *Euclid* and SKAO-like specifications because they are quite different between each other as detailed in the following section. Then we will be able to show how the forecasts can actually change. Another survey we could consider is Rubin-LSST but its specifications are more close to the *Euclid* photometric ones.

A. Method

We follow the methodology adopted in Ref. [72], which extends the treatment of the spectroscopic and photometric probes for ΛCDM described in Ref. [73] to scale-independent MG models. We summarize it here.

For the GC_{sp} probe we consider the observed galaxy power spectrum defined as

$$P_{\rm obs}(k,\mu_\theta;z) = \frac{1}{q_\perp^2(z)q_\parallel(z)}\left\{\frac{[b\sigma_8(z)+f\sigma_8(z)\mu_\theta^2]^2}{1+[f(z)k\mu_\theta\sigma_{\rm p}(z)]^2}\right\} \times \frac{P_{\rm dw}(k,\mu_\theta;z)}{\sigma_8^2(z)}F_z(k,\mu_\theta;z)+P_{\rm s}(z), \quad (58)$$

where

$$q_\perp(z) = \frac{D_{\rm A}(z)}{D_{\rm A,ref}(z)}, \quad (59)$$

$$q_\parallel(z) = \frac{H_{\rm ref}(z)}{H(z)}, \quad (60)$$

accounts for the Alcock-Paczynski effect, defined in term of the angular diameter distance $D_A(z)$ and the Hubble parameter $H(z)$. The subscript "ref" stands for reference cosmology. The term in the curly bracket accounts for the redshift-space distortions where we define the effective scale-independent galaxy bias b, for which we consider numerical values as in Ref. [73] (in the analysis we consider $\ln(b\sigma_8)$ as a free parameter and we marginalize over), the growth rate, f, and the square of the cosine of the angle between the wave vector $\boldsymbol{k}$ and the line-of-sight direction, μ_θ^2. We note that the denominator includes the finger-of-God effect. We consider $\sigma_{\rm v}^2 = \sigma_{\rm p}^2$, with

$$\sigma_{\rm v}^2(z) = \frac{1}{6\pi^2}\int {\rm d}k P_{\rm L}(k,z), \quad (61)$$

and $P_{\rm L}$ being the linear matter power spectrum. They are evaluated at every redshift bin, and we kept them fixed. Additionally $P_{\rm dw}$ defines the de-wiggled power spectrum, which includes the smearing of the baryon acoustic oscillations, which reads

$$P_{\rm dw}(k,\mu_\theta;z) = P_{\rm L}(k;z){\rm e}^{-g_\mu k^2} + P_{\rm nw}(k;z)(1-{\rm e}^{-g_\mu k^2}), \quad (62)$$

where $P_{\rm nw}$ stands for a no-wiggle power spectrum. Nonlinearities are included in the nonlinear damping factor [74]

$$g_\mu(k,\mu_\theta,z) = \sigma_{\rm v}^2(z)\{1-\mu_\theta^2+\mu_\theta^2[1+f(z)]^2\}. \quad (63)$$

The function F_z accounts for the redshift uncertainty as it is defined as

$$F_z(k,\mu_\theta;z) = {\rm e}^{-k^2\mu_\theta^2\sigma_r^2(z)}, \quad (64)$$

with $\sigma_r^2(z) = (1+z)\sigma_z/H(z)$, and $P_{\rm s}$ takes into account a residual shot noise, and it is considered as a nuisance parameter.

For the photometric probes we consider the angular power spectra, which, under the Limber approximation, reads

$$C_{ij}^{XY}(\ell) = \int_{z_{\rm min}}^{z_{\rm max}} {\rm d}z \frac{W_i^X(z)W_j^Y(z)}{H(z)r^2(z)}P_{\rm NL}(k_\ell,z), \quad (65)$$

where i and j stand for two tomographic bins, and X and Y represent either CG_{ph} or WL, $k_\ell = (\ell+1/2)/r(z)$, and $r(z)$ is the comoving distance. $P_{\rm NL}$ stands for the nonlinear matter power spectrum, which we take from ReACT [see Eq. (52)]. Additionally we define the kernels for galaxy clustering and weak lensing,

$$W_i^{\rm G}(k,z) = b_i(k,z)\frac{n_i(z)}{\bar{n}_i}H(z), \quad (66)$$

$$W_i^{\rm L}(k,z) = \frac{3}{2}\Omega_{\rm m,0}H_0^2(1+z)r(z)\Sigma(z) \times \int_z^{z_{\rm max}} {\rm d}z' \frac{n_i(z')}{\bar{n}_i}\frac{r(z'-z)}{r(z')} + W_i^{\rm IA}(k,z). \quad (67)$$

In these expressions $n_i/\bar{n}_i$ is the normalized number density in the ith bin. The galaxy distribution is binned into 10 equipopulated redshift bins with a true distribution $n(z) \propto (z/z_0)^2 \exp[-(z/z_0)^\gamma]$, with $z_0 = z_m/\sqrt{2}$ being the median redshift, we will specify these numbers in the survey specifications. To account for the photometric redshift uncertainties the redshift distribution is then convolved with a sum of two Gaussian distributions. For details about the expressions see Ref. [73]. Additionally, b_i are the constant values of bias in each bin and are considered as nuisance parameters, then we marginalize over. Their fiducial values are computed as $b_i(z) = \sqrt{1+\bar{z}}$ with $\bar{z}$ being the mean redshift of the bin (in this we follow Ref. [73]). Σ encodes the changes to the lensing potential for MG. In our case $\Sigma = \mu$. Finally $W_i^{\rm IA}$ defines the intrinsic alignment of galaxies with the extended nonlinear alignment model [73]

$$W_i^{\rm IA}(k,z) = -\frac{\mathcal{A}_{\rm IA}\mathcal{C}_{\rm IA}\Omega_{\rm m,0}\mathcal{F}_{\rm IA}(z)}{\delta(k,z)/\delta(k,z=0)}\frac{n_i(z)}{\bar{n}_i(z)}H(z), \tag{68}$$

and

$$\mathcal{F}_{\rm IA}(z) = (1+z)^{\eta_{\rm IA}}\left[\frac{\langle L\rangle(z)}{L_\star(z)}\right]^{\beta_{\rm IA}}. \tag{69}$$

with $\langle L\rangle(z)$ and $L_*(z)$ being the mean and the characteristic luminosity of source galaxies.

We will use specifications of surveys such as *Euclid*-like and SKAO-like, which are very close to the more realistic cases. In detail:

(i) For a *Euclid*-like survey we consider [72,73,75]: a survey area of 15000 deg^2; $N_z = 10$ (number of photo-z bins), $\bar{n}_{\rm gal} = 30$ arcmin^{-2} (galaxy number density), $z_m = 0.9$, $\gamma = 3/2$, $\sigma_\epsilon = 0.3$ (intrinsic ellipticity), $\ell_{\rm min} = 10$ (minimum multipole) for both GC$_{\rm ph}$ and WL and $\ell_{\rm max} = 1500$ (maximum multipole) for WL and $\ell_{\rm max} = 750$ for GC$_{\rm ph}$; for GC$_{\rm sp}$ we adopt $n_z = 4$ (number of spectro-z bins), the centers of the bins are $z_i = \{1.0, 1.2, 1.4, 1.65\}$, the error on redshift is 0.001, the minimum scale $k_{\rm min} = 0.001\ h\,{\rm Mpc}^{-1}$ and the maximum scale is $k_{\rm max} = 0.25\ h\,{\rm Mpc}^{-1}$. These specifications can be considered very close to the real case. To test the power in constraining of the nonlinear scales we also adopt a smaller $k_{\rm max} = 0.15\ h\,{\rm Mpc}^{-1}$ for GC$_{\rm sp}$ and smaller $\ell_{\rm max}$ respectively $\ell_{\rm max} = 500$ for GC$_{\rm ph}$ and $\ell_{\rm max} = 1000$ for WL. We refer to this case as quasilinear (QL).

(ii) For a SKAO-like survey [76]: we consider a survey area of 5000 deg^2; $N_z = 10$, $\bar{n}_{\rm gal} = 2.7$ arcmin^{-2}, $z_m = 1.1$, $\gamma = 1.25$, $\sigma_\epsilon = 0.3$, for $\ell_{\rm min}$ and $\ell_{\rm max}$ as well as for $k_{\rm max}$ we use the same as *Euclid*-like for both spectroscopic and photometric probes.

We use a Fisher matrix approach [77–79] to estimate errors for cosmological and model parameter measurements as implemented in the publicly available library CosmicFish [80,81]. This approach approximates the curvature of the likelihood at the peak, under the assumption that it is a Gaussian function of the model parameters.

For the forecast analysis we will vary the following cosmological parameters around their fiducial values:

$$\Omega_{\rm m} = 0.2565, \quad \Omega_{\rm b} = 0.041, \quad h = 0.737$$
$$n_{\rm s} = 0.96605, \quad \sigma_8 = 0.891, \tag{70}$$

where $\Omega_{\rm m} = \Omega_{\rm c} + \Omega_{\rm b}$ and $h = H_0/100$ and the model parameters which fiducial values are

$$q = 1.06, \quad s = 0.65. \tag{71}$$

The fiducial values have been chosen to be the best fit values for GCCG with *Planck* data obtained in Ref. [24]. For stability reason both $\{q, s\}$ need to be positive. However the use of the Fisher matrix approach to compute the constraints does not allow us to impose *a priori* such cuts in the parameter space. Therefore while the results assume Gaussianity we will *a posteriori* cut the negative range when presenting our results.

B. Results

We show in Figs. 4 and 5 the 1σ and 2σ contours for the probes GC$_{\rm sp}$, WL, WL + GC$_{\rm ph}$, WL + GC$_{\rm ph}$ + XC and all the combined probes, GC$_{\rm sp}$ + WL + GC$_{\rm ph}$ + XC, respectively for *Euclid*-like and SKAO-like. We also show in Figs. 6 and 7 the 1σ and 2σ contours for the same combinations of probes in the QL case for both surveys. In Table I we list the forecasted 1σ relative errors to its fiducial on the cosmological and model's parameters for the same combinations of probes.

As shown in Table I, for the MG parameter s we find that at 1σ the *Euclid*-like survey has a stronger power in constraining compared to SKAO-like survey. In details, the GC$_{\rm sp}$ for a *Euclid*-like survey will constrain s with a relative error of ∼14.4%, while for SKAO-like survey it is much higher ∼82.5%; in the WL alone case the relative error is ∼67.1% for *Euclid*-like, while for SKAO-like the parameter s is unconstrained; when the WL is combined with GC$_{\rm ph}$ the relative error decreases to 23.5% for *Euclid*-like, while s is still unconstrained for SKAO-like. The error strongly improves when the XC is considered: ∼9.7% and ∼53.4% for *Euclid* and SKAO-like respectively. Finally the full combination gives a further better constraint in the case of *Euclid*-like (∼6.2% relative error) and a slightly worse error for SKAO-like, ∼36.9%. In the SKAO case then the

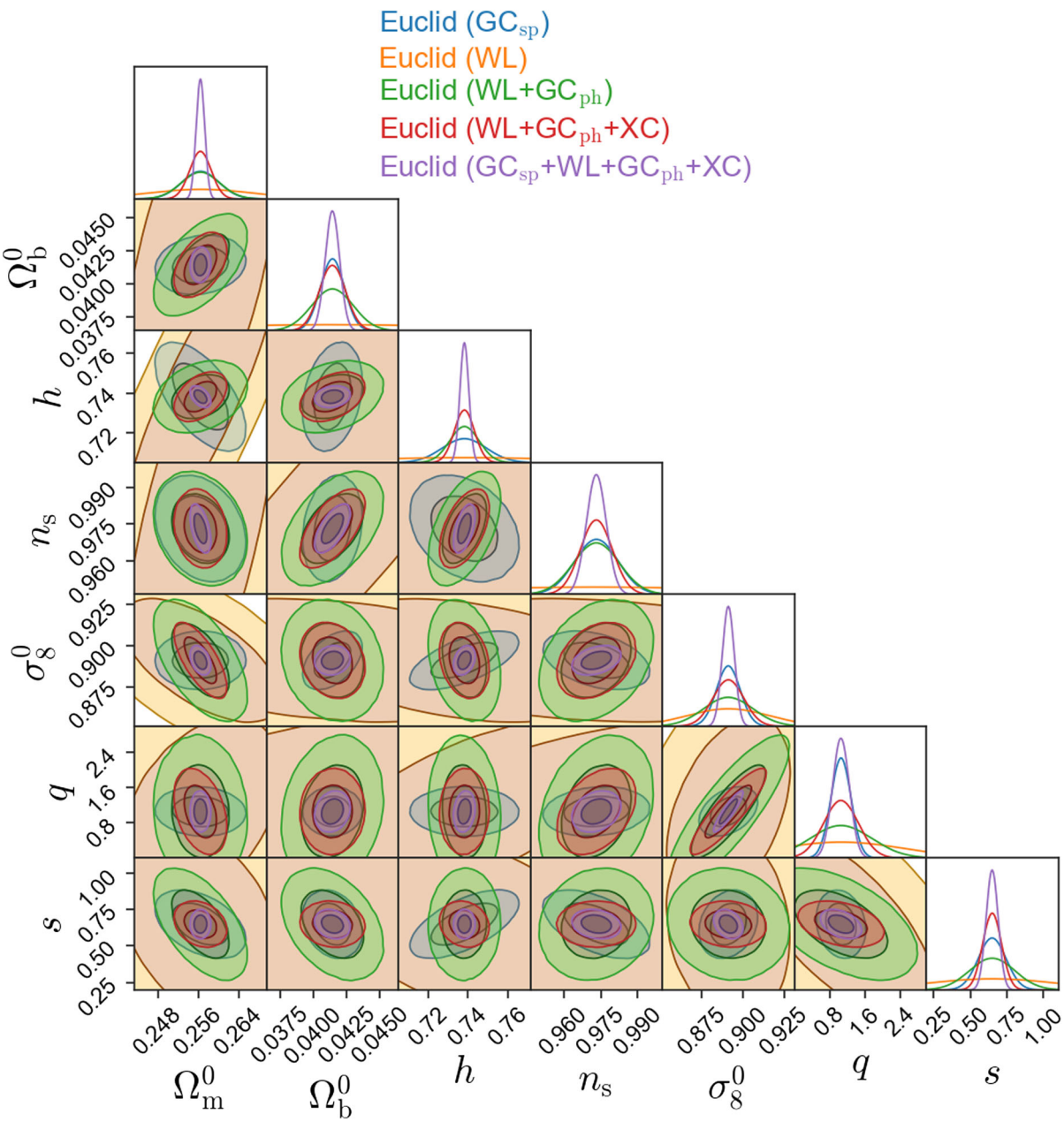

FIG. 4. 1σ and 2σ joint marginalized error contours on the cosmological and GCCG model parameters for a *Euclid*-like survey. Blue is GC_{sp}, orange is for WL, green for the combination WL + GC_{ph}, red for WL + GC_{ph} + XC and magenta for all the photometric probes, including their cross-correlation, combined with GC_{sp}.

cross-correlation between the photometric probes as well as its combination with spectroscopic GC will be crucial to set a constraint on the s parameter.

When we consider the QL specifications for both surveys the constraints on the s parameter become worse, as it can be expected given that we cut the power in constraining coming from the larger k. Specifically with the *Euclid*-like specifications for the spectroscopic probe we obtain ∼93%, for weak lensing ∼87.4% and for WL combined with GC_{ph} we find 40.6%. For SKAO-like these probes alone are not able to constrain s. The combinations with the cross correlation of GC_{ph} and WL largely improve the relative error which is comparable to the one with more realistic specifications (∼14.2 with WL + GC_{ph} + XC and 9.6% for the full combination). For SKAO-like we have 84.3% and 51.5%.

For the MG parameter q, we also find that at 1σ the *Euclid*-like survey performs better compared to the SKAO-like survey. In details, for *Euclid*-like the relative error is ∼21.2% with GC_{sp} while for SKAO-like it is ∼71.8%.

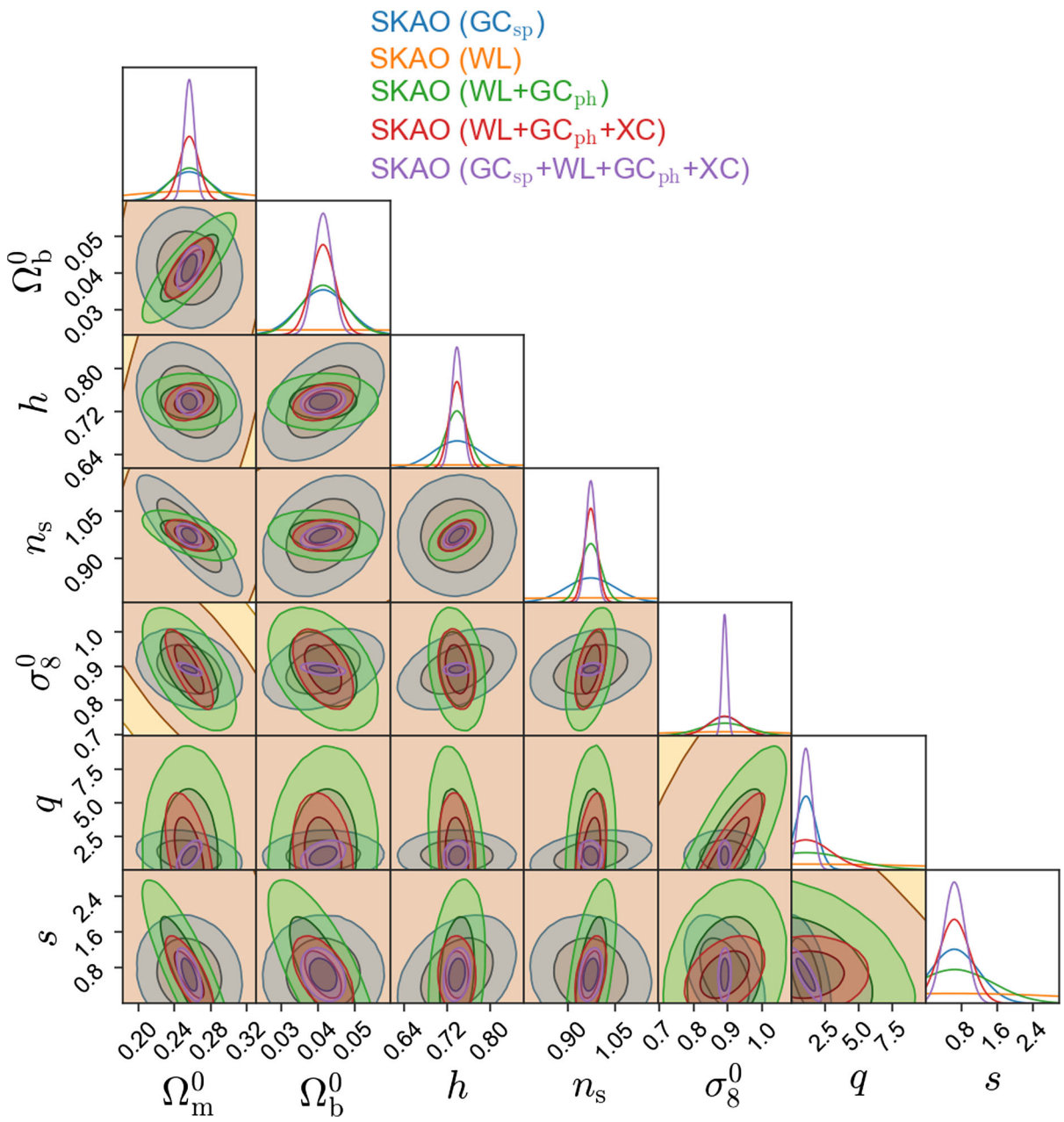

FIG. 5. 1σ and 2σ joint marginalized error contours on the cosmological and GCCG model parameters for an SKAO-like survey. Blue is GC_{sp}, orange is for WL, green for the combination $WL + GC_{ph}$, red for $WL + GC_{ph} + XC$ and magenta for all the photometric probes, including their cross-correlation, combined with GC_{sp}.

For both surveys WL alone is not able to constrain the parameter q. In the case of *Euclid*-like the combination of $WL + GC_{ph}$ improves the error which is 65.1%, while for SKAO-like the inclusion of the photometric galaxy clustering probe does not make any difference. Finally the inclusion of the XC in the photometric probes for the *Euclid*-like survey gives an even better constraint ∼36.9% and the strongest constraint is ∼17.7% for the full combination. For SKAO-like we obtain a constraint ∼43.5% only for the full combination. In the QL regime *Euclid*-like loses its power in constraining for both the spectroscopic and photometric GC, while the errors when the XC is included increase (∼75.4% with $WL + GC_{ph} + XC$ and ∼23% for the full combination), but still performs better than SKAO-like. In the SKAO-like we get a constraint only in the full combination of probes give the orthogonality of the spectroscopic and photometric probes, see Fig. 7.

In Table I we show also the forecasts on the cosmological parameters $\{\Omega_m^0, \Omega_b^0, h, n_s\sigma_8^0\}$. We can see how the *Euclid*-like survey performs very well on all parameters

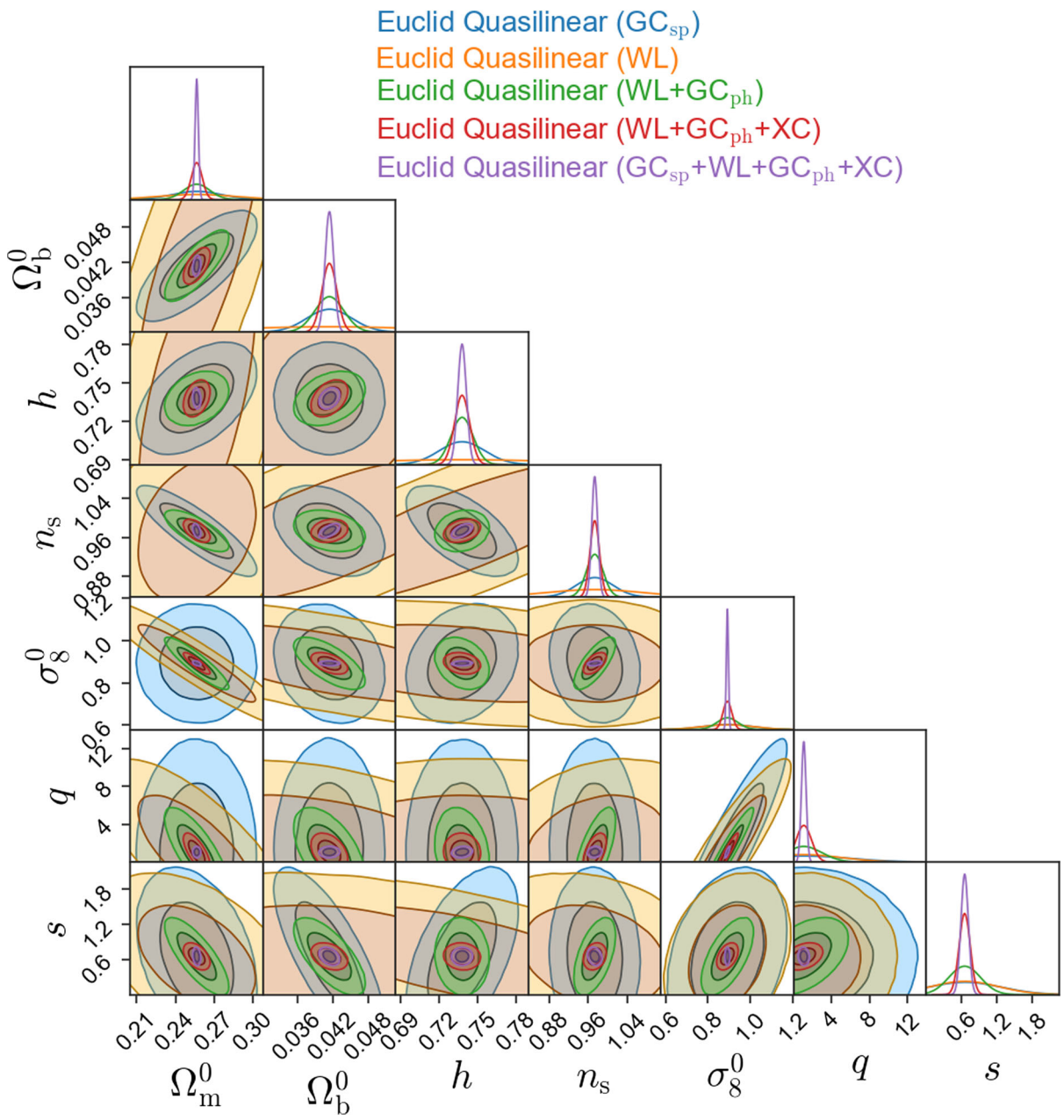

FIG. 6. 1σ and 2σ joint marginalized error contours on the cosmological and GCCG model parameters for a *Euclid*-like survey when quasilinear cuts to linear and angular scales are applied. Blue is $\mathrm{GC_{sp}}$, orange is for WL, green for the combination $\mathrm{WL}+\mathrm{GC_{ph}}$, red for $\mathrm{WL}+\mathrm{GC_{ph}}+\mathrm{XC}$ and magenta for all combination of probes.

and for all the combinations of probes considered. The only parameter with a larger relative error is Ω_b^0, ∼25.5% for WL alone, but this is usually also the case of ΛCDM [73]. In the SKAO-like case the constraints are all worse with respect to the *Euclid*-like case. In the QL case the constraints degrade for both surveys with *Euclid*-like case performing in any case better than SKAO. Comparing our forecast on the cosmological parameters with those of the ΛCDM obtained for *Euclid* in [73] (see Table 9 pessimistic case) we notice that the order of magnitude of the errors is the same as we find in this work, with GCCG performing slightly better on some parameters and for some probes. While this is surprising, because in general the inclusion of additional parameters with respect to the baseline ones leads to larger errors, we attribute this different tendency here to the presence of the parameter s at level of the background which affects the constraints on cosmological parameters. Indeed from Fig. 4 in the bottom line, we can notice that the orientation of the ellipses of the spectroscopic and photometric probes

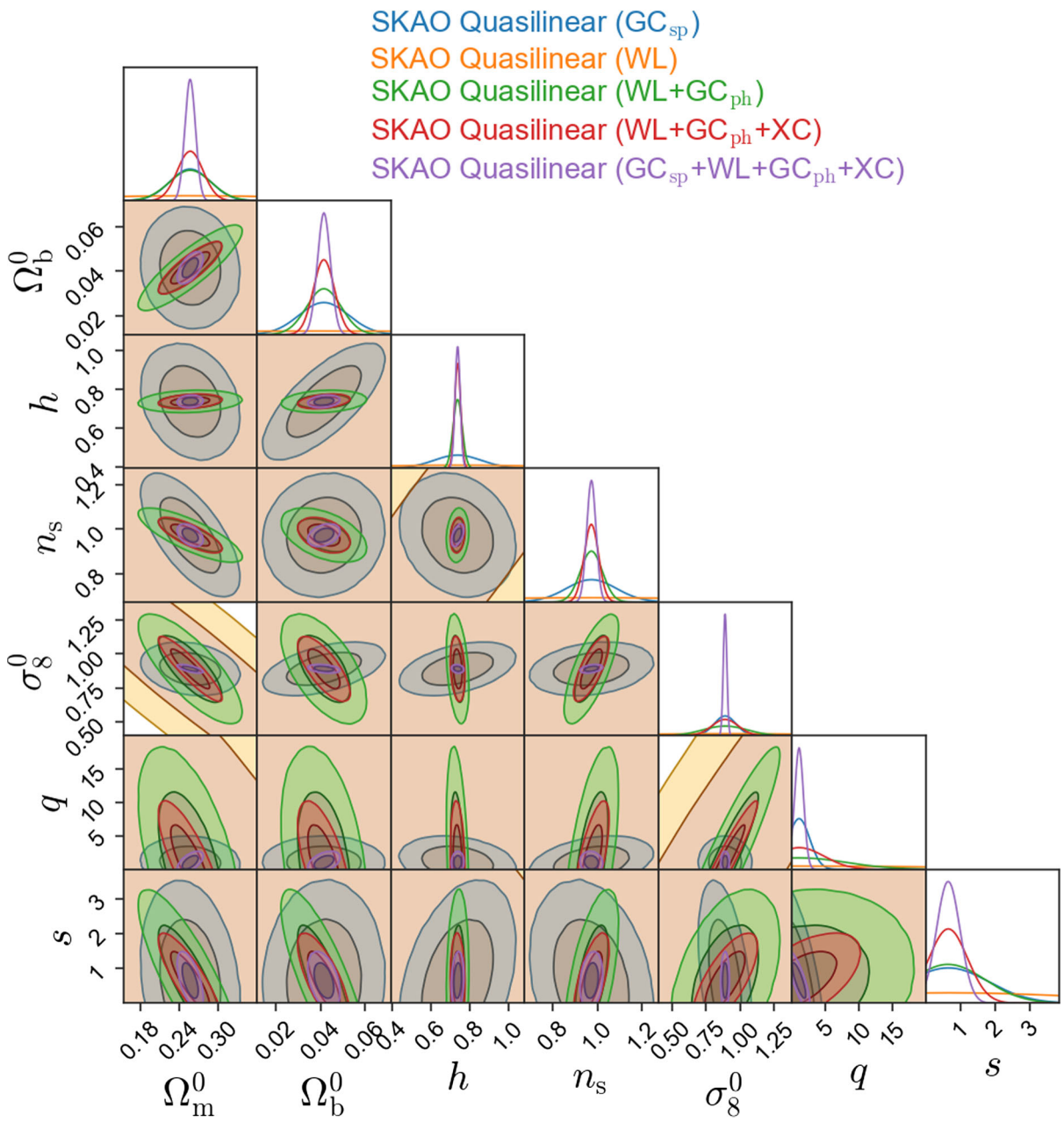

FIG. 7. 1σ and 2σ joint marginalized error contours on the cosmological and GCCG model parameters for a SKAO-like survey when quasilinear cuts to linear and angular scales are applied. Blue is GC_{sp}, orange is for WL, green for the combination $WL + GC_{ph}$, red for $WL + GC_{ph} + XC$ and magenta for all the photometric probes, including their cross-correlation, combined with GC_{sp}.

TABLE I. Marginalized 1σ relative errors on the cosmological and GCCG model parameters using *Euclid*-like and SKAO-like specifications for spectroscopic galaxy clustering (GC_{sp}), weak lensing (WL), photometric galaxy clustering (GC_{ph}) and the cross-correlation between the photometric probes (XC).

Data	Ω_m^0 (%)	Ω_b^0 (%)	h (%)	n_s (%)	σ_8^0 (%)	q (%)	s (%)
Euclid (GC_{sp})	1.4	2.2	1.5	0.9	0.8	21.2	14.4
Euclid (WL)	4.0	25.5	7.1	6.7	2.8	132.2	67.1
Euclid ($WL + GC_{ph}$)	1.4	3.7	1.0	1.0	1.7	65.1	23.5
Euclid ($WL + GC_{ph} + XC$)	0.8	2.4	0.7	0.7	1.0	36.9	9.7
Euclid ($GC_{sp} + WL + GC_{ph} + XC$)	0.3	1.3	0.3	0.4	0.4	17.7	6.2

(Table continued)

TABLE I. *(Continued)*

Data	Ω_m^0 (%)	Ω_b^0 (%)	h (%)	n_s (%)	σ_8^0 (%)	q (%)	s (%)
Euclid quasilinear (GC_{sp})	7.2	9.0	2.4	3.8	12.5	449.6	93.0
Euclid quasilinear (WL)	11.6	38.6	11.1	9.9	13.4	370.2	87.4
Euclid quasilinear ($WL + GC_{ph}$)	3.9	5.8	1.1	1.7	5.5	177.0	40.6
Euclid quasilinear ($WL + GC_{ph} + XC$)	1.6	3.0	0.8	1.0	2.3	75.4	14.2
Euclid quasilinear ($GC_{sp} + WL + GC_{ph} + XC$)	0.5	1.7	0.4	0.6	0.5	23.0	9.6
SKAO (GC_{sp})	9.1	16.0	6.0	7.9	5.3	71.8	82.5
SKAO (WL)	27.2	146.2	46.0	42.8	24.3	920.8	440.5
SKAO ($WL + GC_{ph}$)	8.1	14.6	2.9	3.3	8.1	307.2	131.6
SKAO ($WL + GC_{ph} + XC$)	4.1	8.0	1.9	2.1	5.3	176.5	53.4
SKAO ($GC_{sp} + WL + GC_{ph} + XC$)	2.2	5.9	1.4	1.6	0.9	43.5	36.9
SKAO quasilinear (GC_{sp})	11.9	26.4	16.4	11.5	8.8	147.2	177.6
SKAO quasilinear (WL)	74.8	239.8	69.7	59.2	84.4	2246.8	605.0
SKAO quasilinear ($WL + GC_{ph}$)	12.4	18.5	3.2	5.0	18.0	646.3	161.3
SKAO quasilinear ($WL + GC_{ph} + XC$)	7.6	11.3	2.1	3.3	10.7	343.7	84.3
SKAO quasilinear ($GC_{sp} + WL + GC_{ph} + XC$)	3.1	7.0	1.8	2.1	1.4	61.7	51.5

are such that their combination may help in reducing the errors.

VII. CONCLUSION

In this work we have presented the nonlinear modeling of the matter power spectrum in the generalized cubic covariant Galileon with the aim of exploiting the constraining power of future surveys. To this extent, we created a new patch for the ReACT code which implements the halo-model reaction prescription. For our model we implemented the modified background evolution, the spherical collapse and the potential energy obtained from the virial theorem. Additionally we included the 1-loop corrections to compute the 1-loop matter power spectra. We demonstrated the performance of this new tool by comparing our theoretical prediction against N-body simulations and we found agreement within 5%.

Finally we focused on the ability of future missions such as *Euclid* and SKAO to constrain the GCCG model parameters. We found that a survey such as *Euclid* will be able to provide outstanding constraints on the two parameters of the model $\{q, s\}$, especially when a larger range of nonlinear scales is considered. We also provide constraints for SKAO which are weaker for both parameters when compared to *Euclid*.

In conclusion, with the tool presented in this work it will be possible to obtain reliable and accurate constraints on the GCCG model with forthcoming surveys. We are confident that when the new data will be available it will allow to discern the GCCG model from ΛCDM.

ACKNOWLEDGMENTS

We thank M. Martinelli and F. Pace for useful discussion. L. A. is supported by Fundação para a Ciência e a Tecnologia (FCT) through the research Grants No. UIDB/04434/2020 and No. UIDP/04434/2020 and from the FCT PhD fellowship grant with Ref. Number 2022.11152.BD. N. F. is supported by the Italian Ministry of University and Research (MUR) through the Rita Levi Montalcini project "Tests of gravity on cosmic scales" with reference PGR19ILFGP. L. A. and N. F. also acknowledge the FCT project with ref. number PTDC/FIS-AST/0054/2021 and the COST Action CosmoVerse, CA21136, supported by COST (European Cooperation in Science and Technology). B. B. is supported by a UKRI Stephen Hawking Fellowship (EP/W005654/2). We are particularly in debt with A. Barreira for collaboration in the early stages of the work.

[1] S. Weinberg, Rev. Mod. Phys. **61**, 1 (1989).
[2] S. M. Carroll, Living Rev. Relativity **4**, 1 (2001).
[3] H. E. S. Velten, R. F. vom Marttens, and W. Zimdahl, Eur. Phys. J. C **74**, 3160 (2014).
[4] A. Joyce, B. Jain, J. Khoury, and M. Trodden, Phys. Rep. **568**, 1 (2015).
[5] A. G. Riess, S. Casertano, W. Yuan, L. M. Macri, and D. Scolnic, Astrophys. J. **876**, 85 (2019).

[6] K. C. Wong *et al.*, Mon. Not. R. Astron. Soc. **498**, 1420 (2020).
[7] W. L. Freedman *et al.*, Astrophys. J. **882**, 34 (2019).
[8] E. Di Valentino *et al.*, Astropart. Phys. **131**, 102605 (2021).
[9] K. Kuijken *et al.*, Mon. Not. R. Astron. Soc. **454**, 3500 (2015).
[10] J. T. A. de Jong *et al.*, Astron. Astrophys. **582**, A62 (2015).
[11] H. Hildebrandt *et al.*, Mon. Not. R. Astron. Soc. **465**, 1454 (2017).
[12] E. Di Valentino *et al.*, Astropart. Phys. **131**, 102604 (2021).
[13] Y. Akrami *et al.* (CANTATA Collaboration), *Modified Gravity and Cosmology: An Update by the CANTATA Network*, edited by E. N. Saridakis, R. Lazkoz, V. Salzano, P. Vargas Moniz, S. Capozziello, J. Beltrán Jiménez, M. De Laurentis, and G. J. Olmo (Springer, New York, NY, 2021).
[14] G. W. Horndeski, Int. J. Theor. Phys. **10**, 363 (1974).
[15] A. Nicolis, R. Rattazzi, and E. Trincherini, Phys. Rev. D **79**, 064036 (2009).
[16] C. Deffayet, G. Esposito-Farese, and A. Vikman, Phys. Rev. D **79**, 084003 (2009).
[17] C. Deffayet, S. Deser, and G. Esposito-Farese, Phys. Rev. D **80**, 064015 (2009).
[18] T. Kobayashi, M. Yamaguchi, and J. Yokoyama, Prog. Theor. Phys. **126**, 511 (2011).
[19] P. Creminelli and F. Vernizzi, Phys. Rev. Lett. **119**, 251302 (2017).
[20] T. Baker, E. Bellini, P. G. Ferreira, M. Lagos, J. Noller, and I. Sawicki, Phys. Rev. Lett. **119**, 251301 (2017).
[21] J. M. Ezquiaga and M. Zumalacárregui, Phys. Rev. Lett. **119**, 251304 (2017).
[22] B. P. Abbott *et al.* (LIGO Scientific, Virgo, Fermi-GBM, and INTEGRAL Collaborations), Astrophys. J. Lett. **848**, L13 (2017).
[23] S. Peirone, G. Benevento, N. Frusciante, and S. Tsujikawa, Phys. Rev. D **100**, 063540 (2019).
[24] N. Frusciante, S. Peirone, L. Atayde, and A. De Felice, Phys. Rev. D **101**, 064001 (2020).
[25] A. De Felice and S. Tsujikawa, J. Cosmol. Astropart. Phys. 02 (2012) 007.
[26] J. Renk, M. Zumalacarregui, F. Montanari, and A. Barreira, J. Cosmol. Astropart. Phys. 10 (2017) 020.
[27] S. Peirone, N. Frusciante, B. Hu, M. Raveri, and A. Silvestri, Phys. Rev. D **97**, 063518 (2018).
[28] F. Giacomello, A. De Felice, and S. Ansoldi, J. Cosmol. Astropart. Phys. 03 (2019) 038.
[29] C. M. Will, Living Rev. Relativity **17**, 4 (2014).
[30] A. I. Vainshtein, Phys. Lett. **39B**, 393 (1972).
[31] M. Cataneo, L. Lombriser, C. Heymans, A. Mead, A. Barreira, S. Bose, and B. Li, Mon. Not. R. Astron. Soc. **488**, 2121 (2019).
[32] B. Bose, M. Cataneo, T. Tröster, Q. Xia, C. Heymans, and L. Lombriser, Mon. Not. R. Astron. Soc. **498**, 4650 (2020).
[33] B. Bose, M. Tsedrik, J. Kennedy, L. Lombriser, A. Pourtsidou, and A. Taylor, Mon. Not. R. Astron. Soc. **519**, 4780 (2023).
[34] https://github.com/nebblu/ACTio-ReACTio.
[35] C. Deffayet, O. Pujolas, I. Sawicki, and A. Vikman, J. Cosmol. Astropart. Phys. 10 (2010) 026.
[36] T. Kobayashi, M. Yamaguchi, and J. Yokoyama, Phys. Rev. Lett. **105**, 231302 (2010).
[37] A. Barreira, B. Li, C. M. Baugh, and S. Pascoli, J. Cosmol. Astropart. Phys. 11 (2013) 056.
[38] A. Barreira, B. Li, C. M. Baugh, and S. Pascoli, J. Cosmol. Astropart. Phys. 08 (2014) 059.
[39] Y. Takushima, A. Terukina, and K. Yamamoto, Phys. Rev. D **92**, 104033 (2015).
[40] L. Amendola, M. Kunz, and D. Sapone, J. Cosmol. Astropart. Phys. 04 (2008) 013.
[41] R. Bean and M. Tangmatitham, Phys. Rev. D **81**, 083534 (2010).
[42] A. Silvestri, L. Pogosian, and R. V. Buniy, Phys. Rev. D **87**, 104015 (2013).
[43] L. Pogosian, A. Silvestri, K. Koyama, and G.-B. Zhao, Phys. Rev. D **81**, 104023 (2010).
[44] L. Amendola, D. Bettoni, A. M. Pinho, and S. Casas, Universe **6**, 20 (2020).
[45] I. Sawicki and E. Bellini, Phys. Rev. D **92**, 084061 (2015).
[46] F. Schmidt, W. Hu, and M. Lima, Phys. Rev. D **81**, 063005 (2010).
[47] R. Kimura and K. Yamamoto, J. Cosmol. Astropart. Phys. 04 (2011) 025.
[48] E. Bellini, N. Bartolo, and S. Matarrese, J. Cosmol. Astropart. Phys. 06 (2012) 019.
[49] A. Barreira, B. Li, W. A. Hellwing, C. M. Baugh, and S. Pascoli, J. Cosmol. Astropart. Phys. 10 (2013) 027.
[50] N. Frusciante and F. Pace, Phys. Dark Universe **30**, 100686 (2020).
[51] B. S. Wright, A. Sen Gupta, T. Baker, G. Valogiannis, and B. Fiorini (LSST Dark Energy Science Collaboration), J. Cosmol. Astropart. Phys. 03 (2023) 040.
[52] G. Brando, K. Koyama, and H. A. Winther, J. Cosmol. Astropart. Phys. 06 (2023) 045.
[53] I. S. Albuquerque, N. Frusciante, F. Pace, and C. Schimd, Phys. Rev. D **109**, 023535 (2024).
[54] F. Bernardeau, S. Colombi, E. Gaztanaga, and R. Scoccimarro, arXiv:astro-ph/0112551.
[55] F. Bernardeau, S. Colombi, E. Gaztanaga, and R. Scoccimarro, Phys. Rep. **367**, 1 (2002).
[56] K. Koyama, A. Taruya, and T. Hiramatsu, Phys. Rev. D **79**, 123512 (2009).
[57] B. Bose and K. Koyama, J. Cosmol. Astropart. Phys. 08 (2016) 032.
[58] M. Raveri, B. Hu, N. Frusciante, and A. Silvestri, Phys. Rev. D **90**, 043513 (2014).
[59] B. Hu, M. Raveri, N. Frusciante, and A. Silvestri, Phys. Rev. D **89**, 103530 (2014).
[60] R. Takahashi, M. Sato, T. Nishimichi, A. Taruya, and M. Oguri, Astrophys. J. **761**, 152 (2012).
[61] A. Mead, S. Brieden, T. Tröster, and C. Heymans, Mon. Not. R. Astron. Soc. **502**, 1401 (2021).
[62] B. Bose, B. S. Wright, M. Cataneo, A. Pourtsidou, C. Giocoli, L. Lombriser, I. G. McCarthy, M. Baldi, S. Pfeifer, and Q. Xia, Mon. Not. R. Astron. Soc. **508**, 2479 (2021).
[63] P. Carrilho, K. Carrion, B. Bose, A. Pourtsidou, J. C. Hidalgo, L. Lombriser, and M. Baldi, Mon. Not. R. Astron. Soc. **512**, 3691 (2022).

[64] G. Parimbelli, C. Carbone, J. Bel, B. Bose, M. Calabrese, E. Carella, and M. Zennaro, J. Cosmol. Astropart. Phys. 11 (2022) 041.
[65] J. Adamek *et al.* (Euclid Collaboration), J. Cosmol. Astropart. Phys. 06 (2023) 035.
[66] S. Srinivasan, D. B. Thomas, and R. Battye, J. Cosmol. Astropart. Phys. 03 (2024) 039.
[67] S. Srinivasan, D. B. Thomas, F. Pace, and R. Battye, J. Cosmol. Astropart. Phys. 06 (2021) 016.
[68] B. Li, G.-B. Zhao, R. Teyssier, and K. Koyama, J. Cosmol. Astropart. Phys. 01 (2012) 051.
[69] C. Becker, C. Arnold, B. Li, and L. Heisenberg, J. Cosmol. Astropart. Phys. 10 (2020) 055.
[70] A. Barreira, B. Li, A. Sanchez, C. M. Baugh, and S. Pascoli, Phys. Rev. D **87**, 103511 (2013).
[71] M. Cataneo, J. D. Emberson, D. Inman, J. Harnois-Deraps, and C. Heymans, Mon. Not. R. Astron. Soc. **491**, 3101 (2020).
[72] N. Frusciante *et al.* (Euclid Collaboration), arXiv:2306.12368.
[73] A. Blanchard *et al.* (Euclid Collaboration), Astron. Astrophys. **642**, A191 (2020).
[74] D. J. Eisenstein, H.-j. Seo, and M. J. White, Astrophys. J. **664**, 660 (2007).
[75] S. Casas *et al.* (Euclid Collaboration), arXiv:2306.11053.
[76] D. J. Bacon *et al.* (SKA Collaboration), Publ. Astron. Soc. Aust. **37**, e007 (2020).
[77] M. Tegmark, A. J. S. Hamilton, M. A. Strauss, M. S. Vogeley, and A. S. Szalay, Astrophys. J. **499**, 555 (1998).
[78] H.-J. Seo and D. J. Eisenstein, Astrophys. J. **633**, 575 (2005).
[79] H.-J. Seo and D. J. Eisenstein, Astrophys. J. **665**, 14 (2007).
[80] M. Raveri, M. Martinelli, G. Zhao, and Y. Wang, arXiv:1606.06273.
[81] https://cosmicfish.github.io.